Electronic Supporting Information

Hao-Xu Zhang, Qing Peng, and Ya-Dong Li

I. Competition between {211} and {210} planes at the corners of <111> MnS nanowires

Indentations are frequently observed at the corners of <111> nanowires, whether the nanowire is a normal one, or a part of a mushroom (Figure 1f) or a cross (inset of Figure 1h). And as shown in Figure 3l, simulations also indicate the corners are somewhat rounded. Thus it is clear that the {211} sheaths have lost their stability at the corners, giving chances for other types of sheaths to come into play on the typically 10-to-20-nm-wide arena. The types of sheaths, according to the GR and GKC mechanisms, are related to specific planes of MnS. So from the acute angles between [111] direction and the straight parts of the side curves of the [111] nanowires, we can get substantial information about the selectivity for silica sheath formation. Among the eight types of acute angles, as summarized in Table S1, we have found seven types on the highly curved [111] nanowire (inset of Figure 3h, Figure S1), which is part of the cross, and a normal [111] nanowire (Figure S2). From Figure S1 and S2 we can draw the conclusion that {211} and {210} planes are the main competing candidates at the corners of <111> nanowires. According to the crystal structure shown in Figure 1a, SiO_4 clusters may also adsorb on {210} planes by anchoring three legs on the three atoms (Mn3, Mn4, and Mn5) in the same {100} plane and the tail on one of the two atoms (Mn1 and Mn2), which lie in the same {110} plane with Mn3 and Mn4. It must have suffered a higher tension for SiO_4 clusters adsorbed on {210} than {211} planes.

Table S1. The eight types of acute angles between a [111] line in a (11-2) plane and the common lines of the plane with some other planes

Planes	{111}	{211}	{100}	{110}	{210}

Angles	1 – 22.2°	2 – 28.6°	4 – 39.2°	5 – 58.5°	6 – 15.2°
		3 – 73.0°			7 – 50.8°
		4 – 39.2°			8 – 67.8°
		5 – 58.5°			1 – 22.2°

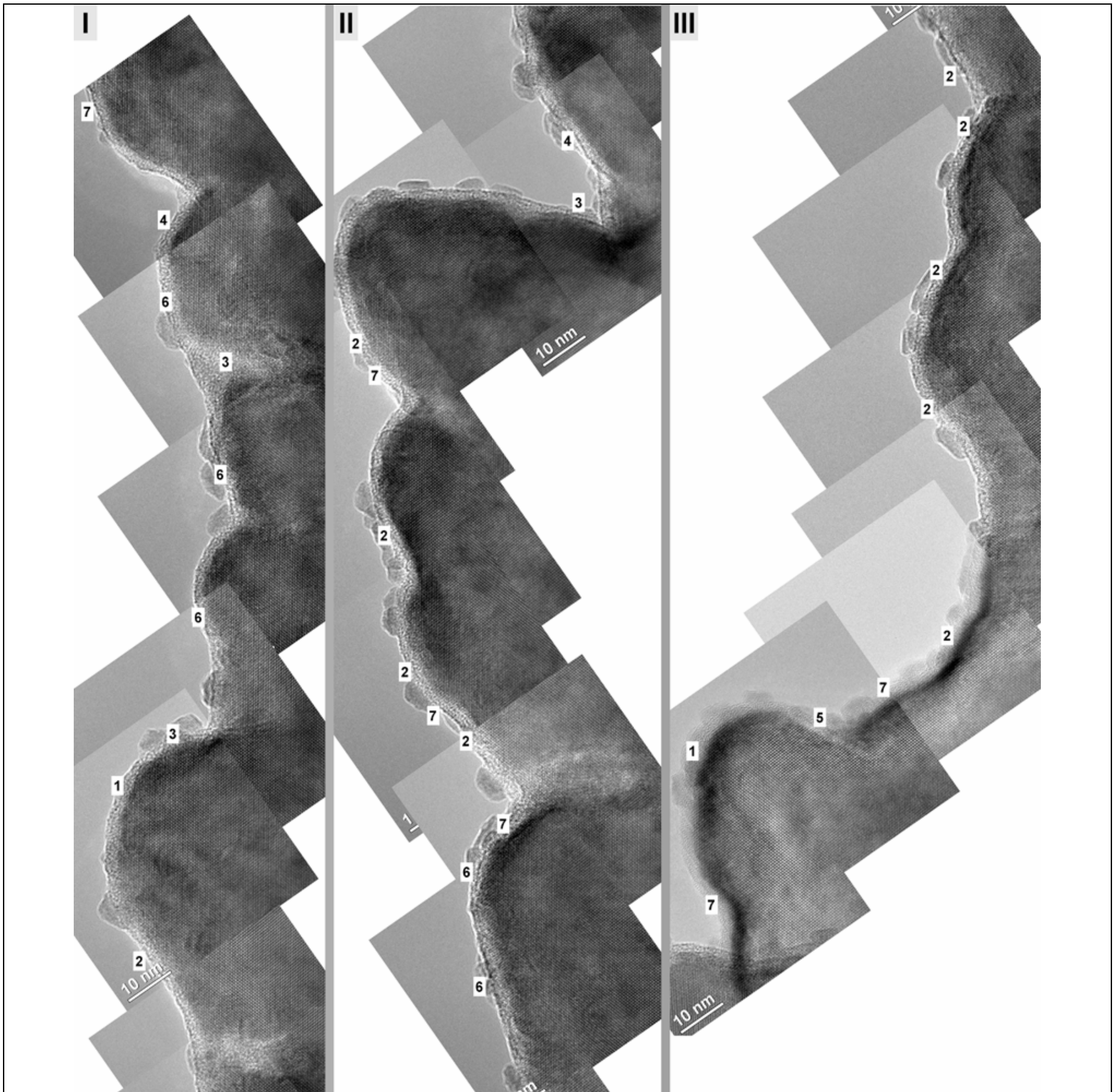

Figure S1. Higher resolution images recorded on the top of the <111> nanowire shown in the inset of Figure 3h.

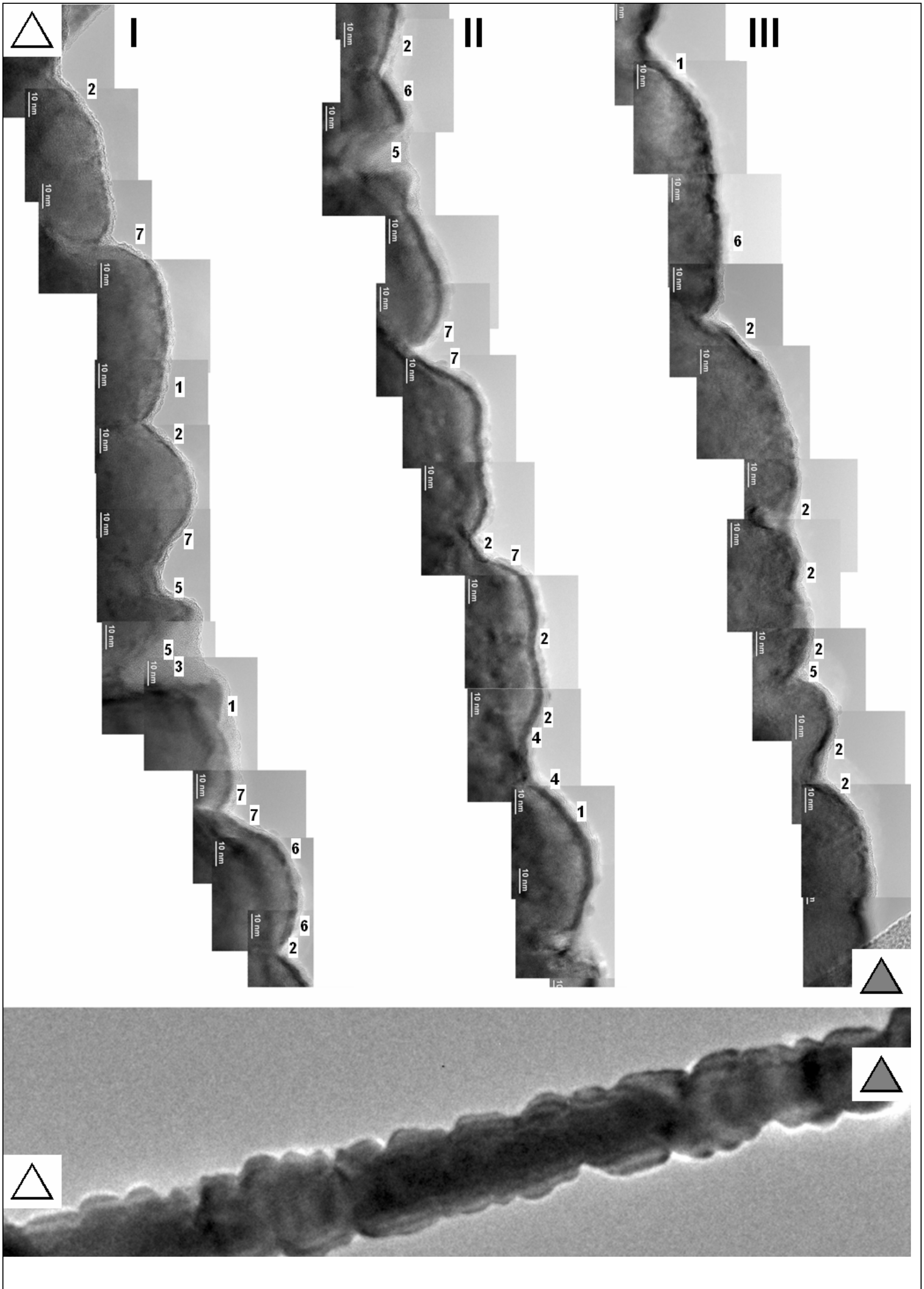
I
2
7
1
2
7
5
5
3
1
7
7
6
6
2
II
2
6
5
7
7
2
7
2
2
4
4
1
III
1
6
2
2
2
2
5
2
2
10 nm

Figure S2. Curves on an <111> MnS nanowire.

II. Highly porous CuCl nanosheets

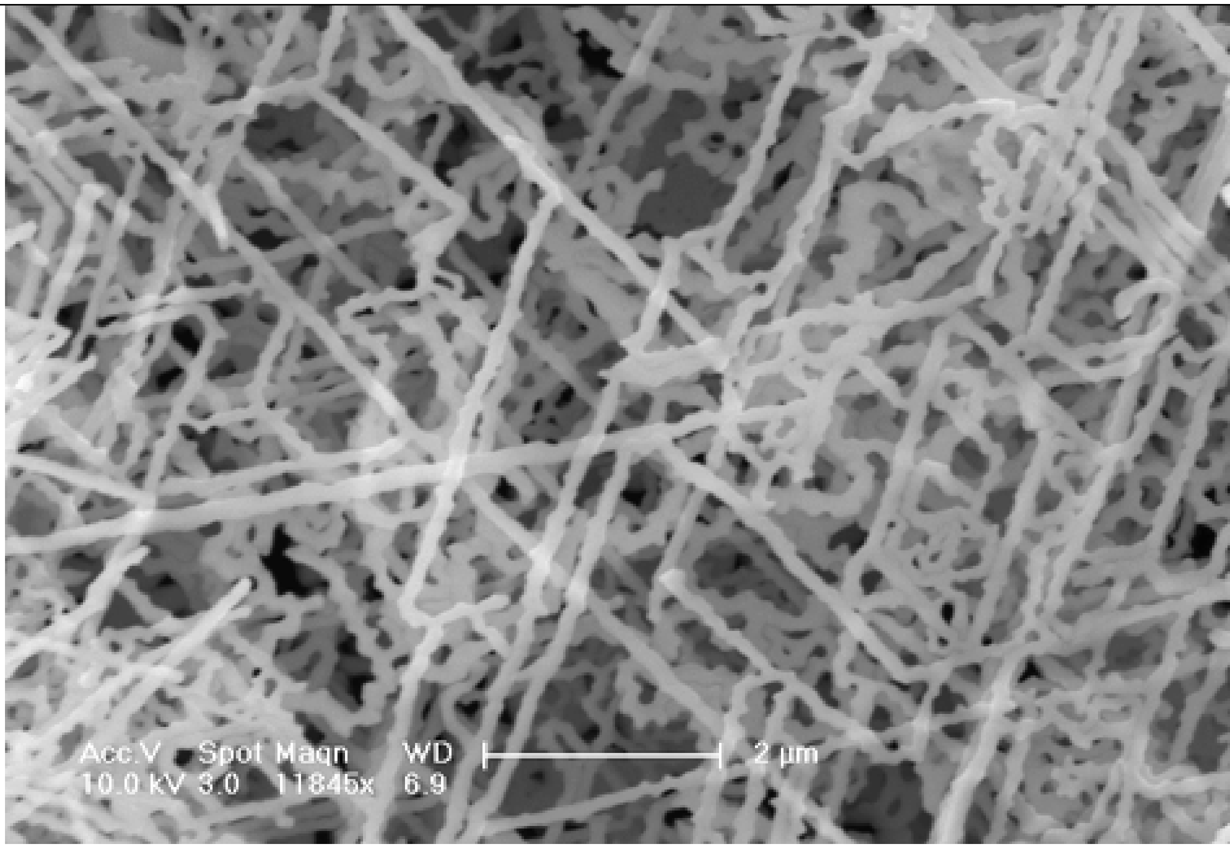

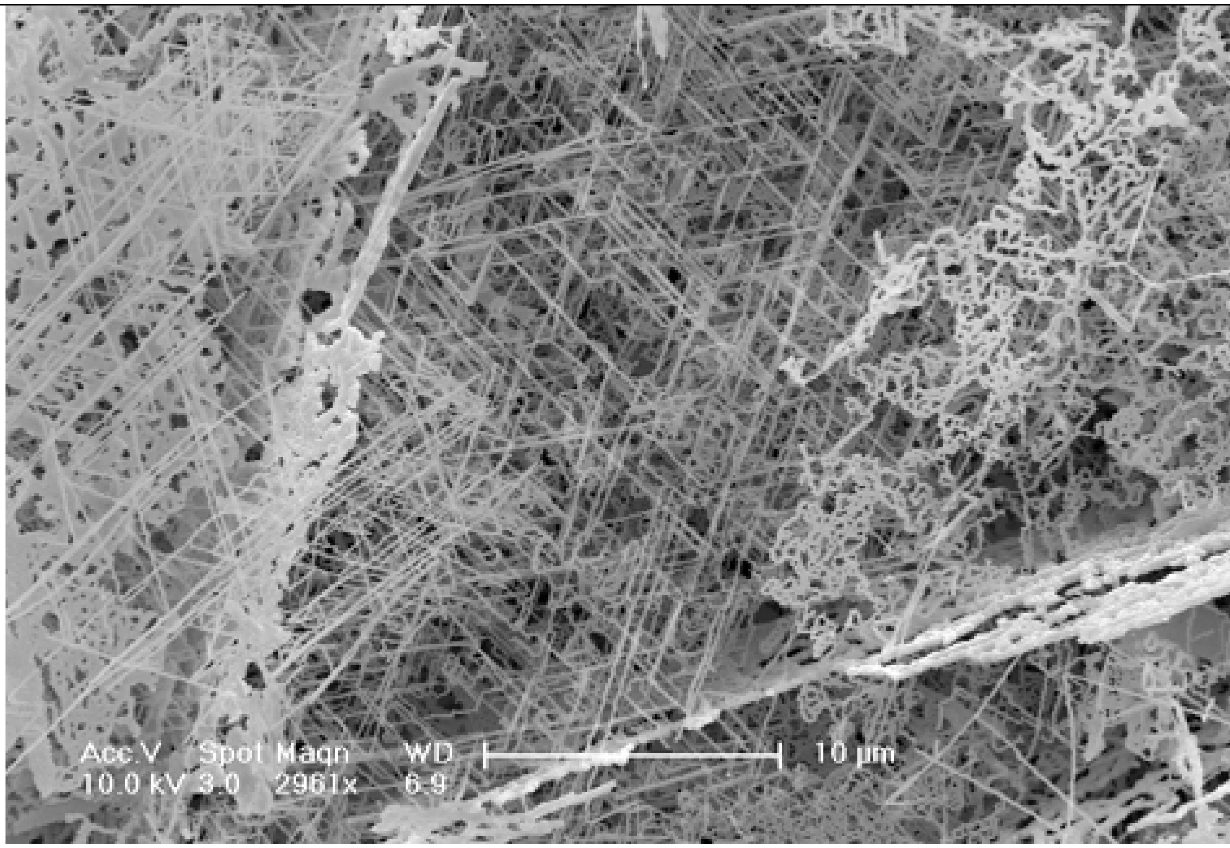
Acc.V Spot Magn WD
10.0 kV 3.0 2961x 6.9
10 μm


Acc.V Spot Magn WD
10.0 kV 3.0 1481x 6.9
20 μm

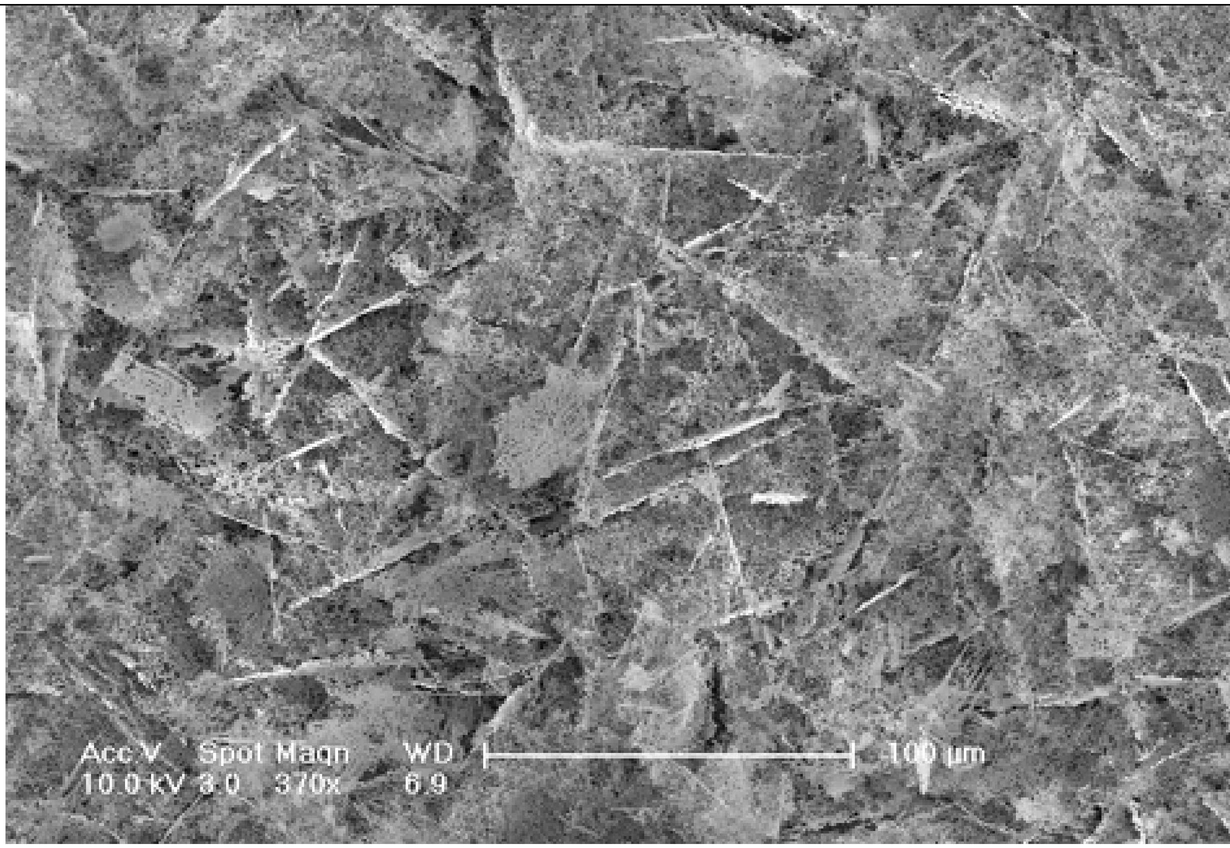

Figure S3. SEM images of highly porous CuCl nanosheets.

III. CuCl platelets prepared under critical supply of $SiCl_4$

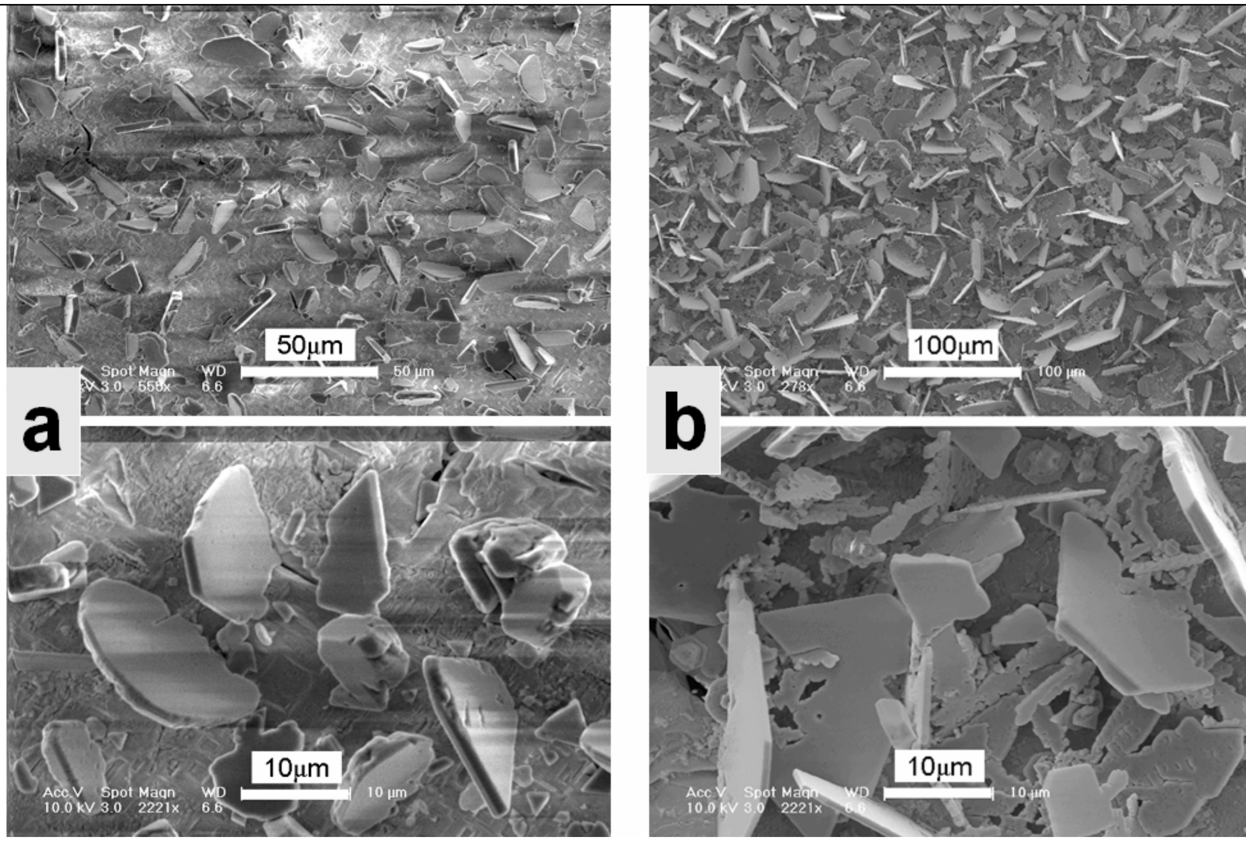

Figure S4. SEM images of silica-sheathed CuCl crystals. In sample (a), about 60% of the products are platelets. The average thickness of the platelets is about 1.5 μm. In sample (b), almost all the products are platelets. The average thickness of the platelets is about 1 μm.

IV. MnSi nanoplatelet

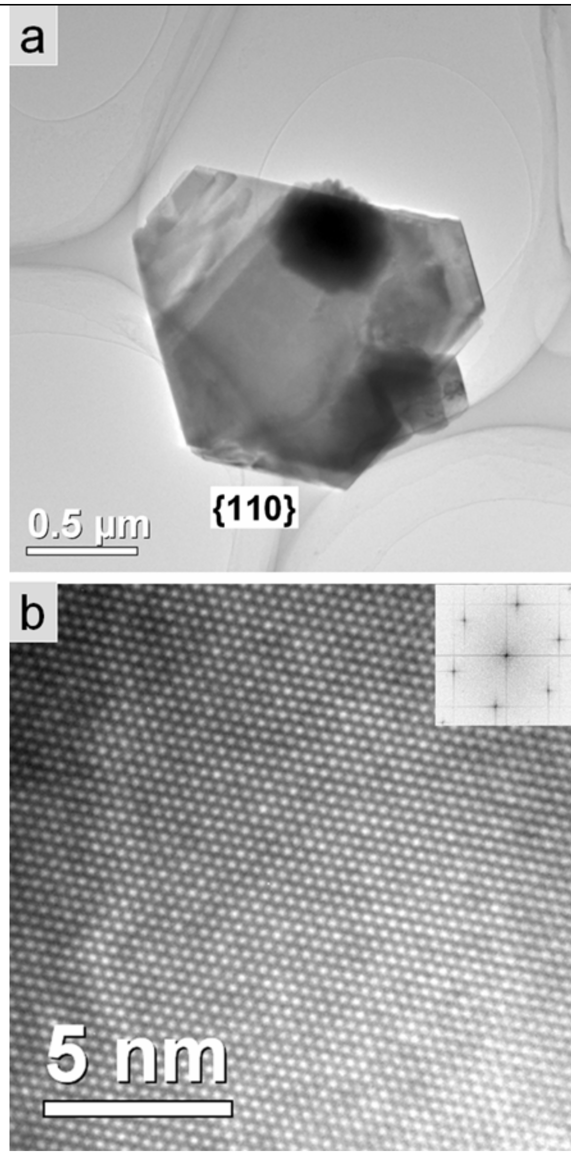

Figure S5. (a) TEM and (b) HRTEM images of a MnSi hexagonal platelet. The inset shows the FFT pattern.

V. Bare CdS and Cu2S nanowires

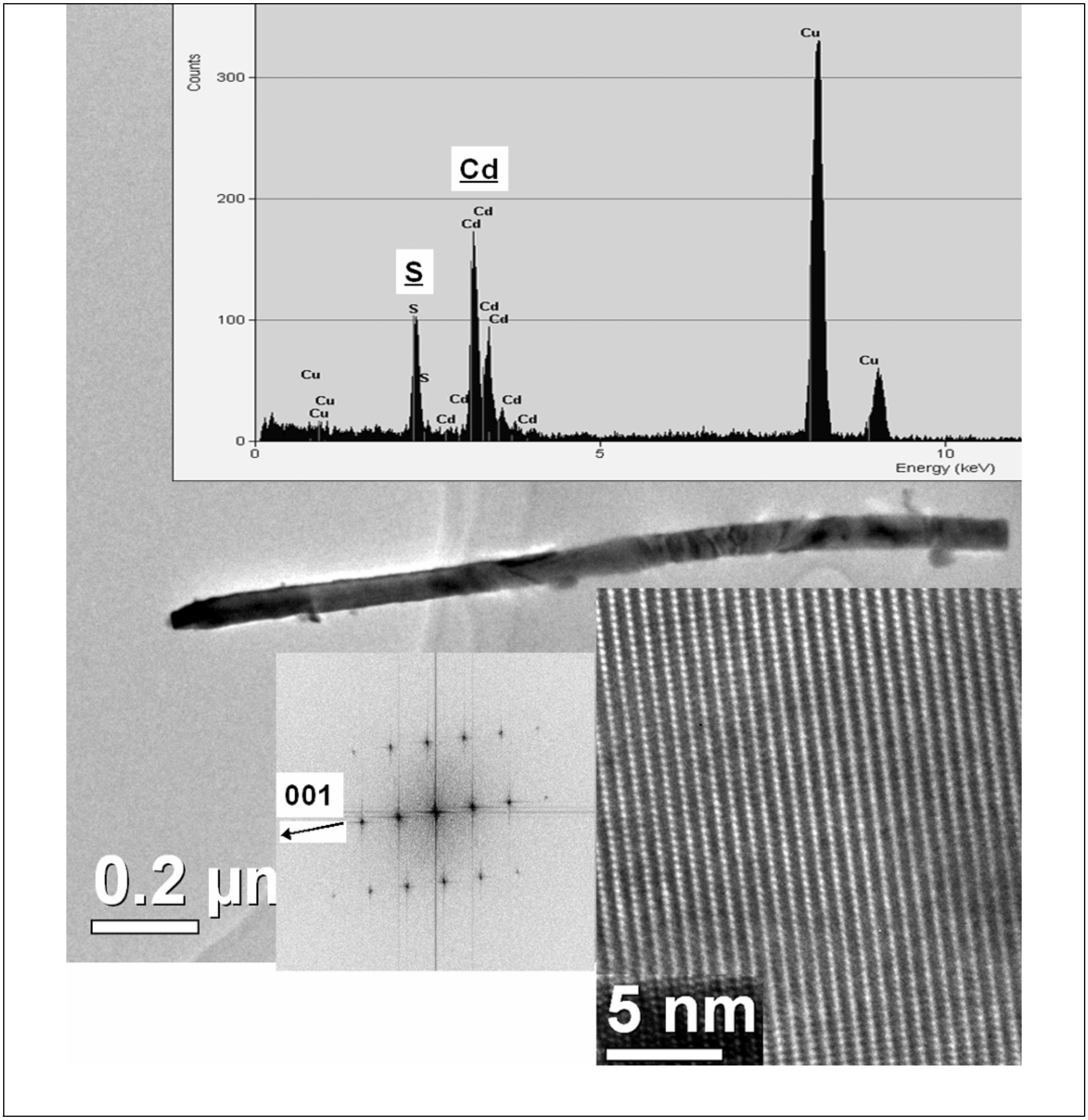
Counts
300
200
100
0
Cd
S
Cu
Cd
Cd
S
Cd
Cd
Cu
S
Cu
Cu
Cd
Cd
Cd
Cd
Cu
0
5
10
Energy (keV)
001
0.2 µm
5 nm

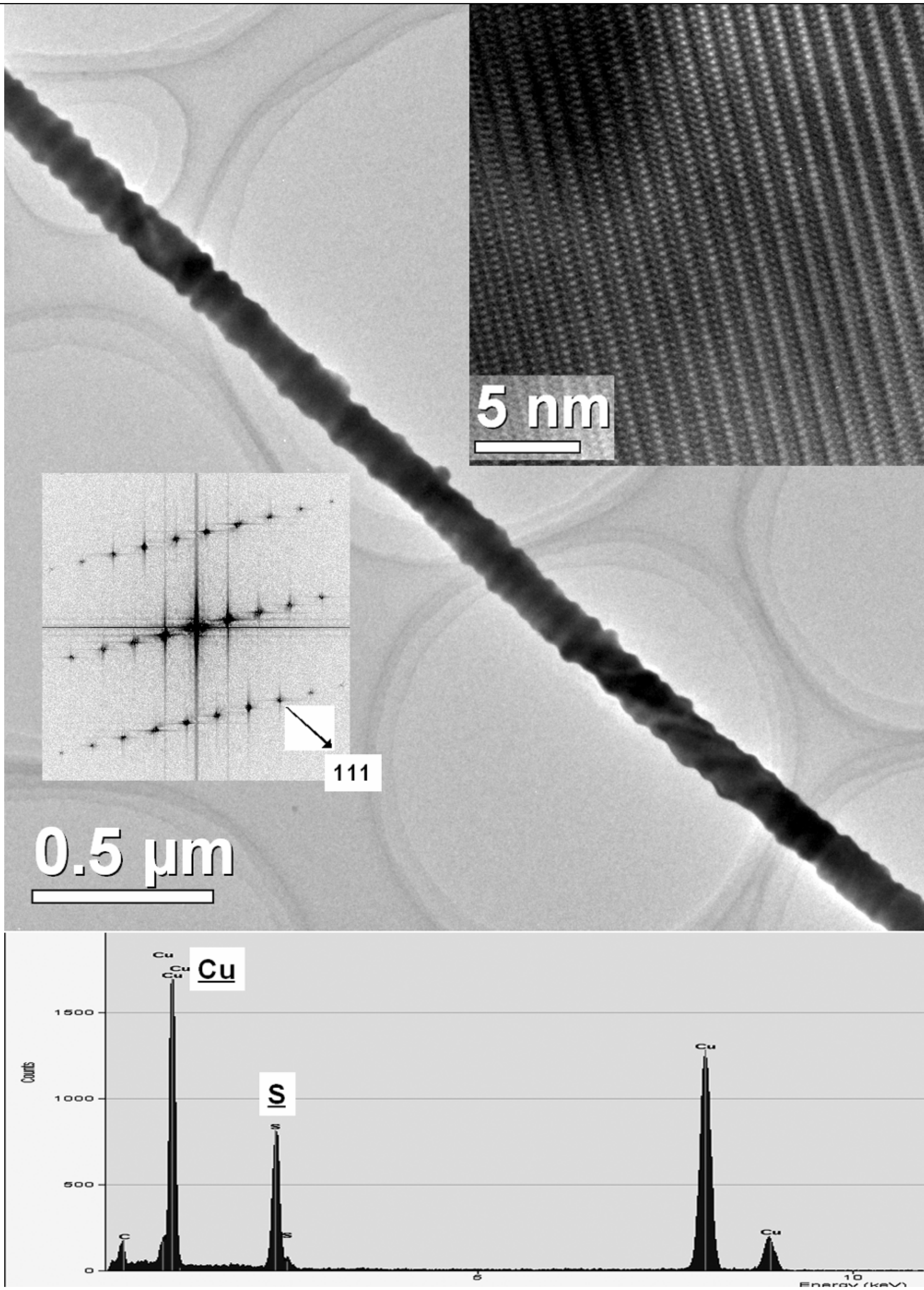
5 nm
111
0.5 µm
Cu
Cu
Cu
Cu
S
S
C
S
Cu
Cu
Counts
1500
1000
500
0
5
10
Energy (keV)

Figure S6. TEM characterization of bare (a) CdS and (b) Cu_2S nanowires. The silica sheaths were removed with hydrofluoric acid. The EDX results confirm the absence of Si element in the cores of the original products.